Powder Technology 191 (2009) 176–181

Contents lists available at ScienceDirect

Powder Technology

journal homepage: www.elsevier.com/locate/powtec

On the formation of phases by mechanical alloying and their thermal stability in Al–Mn–Ce system

S. Mula, S. Ghosh, S.K. Pabi *

Metallurgical and Materials Engineering Department, Indian Institute of Technology, Kharagpur-721 302, India

ARTICLE INFO

Article history:
Received 7 May 2008
Received in revised form 24 August 2008
Accepted 1 October 2008
Available online 11 October 2008

Keywords:
Nanostructures
Intermetallic compound
Amorphization
Transmission electron microscopy (TEM)
Differential scanning calorimetry (DSC)

ABSTRACT

The nanostructured phases formed in the elemental powder blends of nominal compositions $Al_{92}Mn_6Ce_2$ and $Al_{93}Mn_6Ce_1$ during mechanical alloying were investigated by X-ray diffraction and transmission electron microscopy. The difference in Ce content in the two alloys strongly influenced the types of the intermetallic phase(s) formation, including those of the Ce-free phases. Partial amorphization observed in $Al_{92}Mn_6Ce_2$ after prolonged (60 h) milling was not apparent in the lower Ce bearing alloy. Analysis of the X-ray diffraction data of these alloys along with those reported in the literature indicated the dominant role of the topological factors in the amorphous phase formation by mechanical alloying of the concerned system. The phases present in the mechanically alloyed $Al_{92}Mn_6Ce_2$ were entirely different from those reported for rapid solidification processing of the same composition [A. Inoue, Nanostruct. Mater. 6 (1995) 53–64.]. Moreover, the phases present in the mechanically alloyed powder showed inferior thermal stability, when compared to that reported for the rapidly solidified product, apparently due to the difference in the nature of structural disorders and strain induced in the products by the two non-equilibrium processing routes.

1. Introduction

Aluminium-based bulk metallic glasses or composites with high specific strengths are eagerly awaited in the transportation and aviation industries [2,3]. The strength of light weight Al alloys could be significantly enhanced from about 600 MPa in the age hardened condition to over 1500 MPa in the amorphous-based alloys or nanocomposites [4]. Synthesis of nanocomposites consisting of amorphous and nanocrystalline phases by mechanical alloying (MA) or rapid solidification processing (RSP) was reported earlier by many researchers [5–14].

Three major factors contributing to the glass formation are the atomic size mismatch, high negative heat of mixing, and multicomponent alloy system [15]. One of the distinct features possessed by the nanostructure produced by MA, compared with those produced by RSP, is the presence of a high level of internal stress in the former [16].

RSP of an alloy having a nominal composition[1] of $Al_{92}Mn_6Ce_2$ is known to generate a unique structure of nanocomposite consisting of nanoscale icosahedral (I) particles surrounded by a thin Al-rich phase [1]. The present paper reports the phase evolution in an elemental blend of the same composition during MA, studied by X-ray diffraction (XRD) and transmission electron microscopy (TEM). Moreover, in an attempt to understand the role of Ce in this system, the MA characteristics of a similar composition containing less amount of Ce, *i.e.*, $Al_{93}Mn_6Ce_1$, were compared with those of $Al_{92}Mn_6Ce_2$. The thermal stability of the amorphous phase produced by MA was also investigated by differential scanning calorimetry (DSC) and was compared with that reported for the product of RSP of the same composition.

2. Experimental

Elemental powders of pure (>99.0 wt.%) Al, Mn and Ce having average particle sizes <70 μm were blended under protective atmosphere to obtain the nominal compositions of $Al_{92}Mn_6Ce_2$ and $Al_{93}Mn_6Ce_1$. The powder blends were subjected to high energy ball milling in the cemented carbide grinding media at a mill speed of 300 rpm. by means of a Fritsch Pulverisette-5 planetary ball mill. The ball to powder weight ratio was 10:1 and toluene was used as the process control agent. The phase evolution with the progress of milling was studied by means of a Philip's X'pert Pro high-resolution X-ray diffractometer using the Co-Kα radiation (λ=0.178897 nm). The refined values of lattice parameter of the Al-rich solid solution (a_{Al}) were calculated from the peak positions in the XRD patterns by the extrapolation of a_{Al} against ($\cos^2\theta/\sin\theta$) to $\cos\theta=0$ [17]. The average crystallite size and lattice microstrain of the Al-rich solid solution were estimated from the broadening of Al_{111} reflection after stripping its $K\alpha_2$ component using Philips X'Pert Plus software, and then analyzing the resultant XRD peak profile by the Voigt method [18], which allowed judicious elimination of the contribution due to the instrumental peak broadening. For the overlapping peaks, the full widths at half-intensity maximum and the true Bragg angle (2θ) were determined by an appropriate deconvolution exercise. A JEOL JEM-2100 transmission electron microscope was employed to observe the

* Corresponding author. Tel.: +91 3222 283272; fax: +91 3222 282280.
E-mail address: skpabi@metal.iitkgp.ernet.in (S.K. Pabi).

[1] All the compositions are expressed in atom % unless otherwise stated.

0032-5910/$ – see front matter © 2008 Elsevier B.V. All rights reserved.
doi:10.1016/j.powtec.2008.10.002

particle size and to establish the crystalline/amorphous nature of the milled samples.

The extent of WC contamination in the mechanically alloyed powders, due to the milling media, was determined by energy dispersive X-ray (EDX) analysis of elemental W at several areas of the sample using a scanning electron microscope (Zeiss, Supra-40), which was fitted with an EDX attachment. The total carbon (C) and oxygen (O) levels in the as-milled powder were determined by elemental analysis using carbon analyzer (LECO, CS-244) and oxygen analyzer (LECO, TC-436), respectively.

The thermal stability of the mechanically alloyed product was characterized by means of a differential scanning calorimeter (Perkin Elmer-Pyris Diamond). The as-milled powder product containing amorphous phase was carefully wrapped up in a thin Al foil and annealed at 250 °C for 2 h in high purity (impurity level <10 ppm) helium atmosphere and the resultant phase transformations were examined by XRD.

3. Results and discussion

Fig. 1(a) shows the modulation of the XRD patterns of $Al_{92}Mn_6Ce_2$ powder blend with the progress of MA. It was interesting to note that

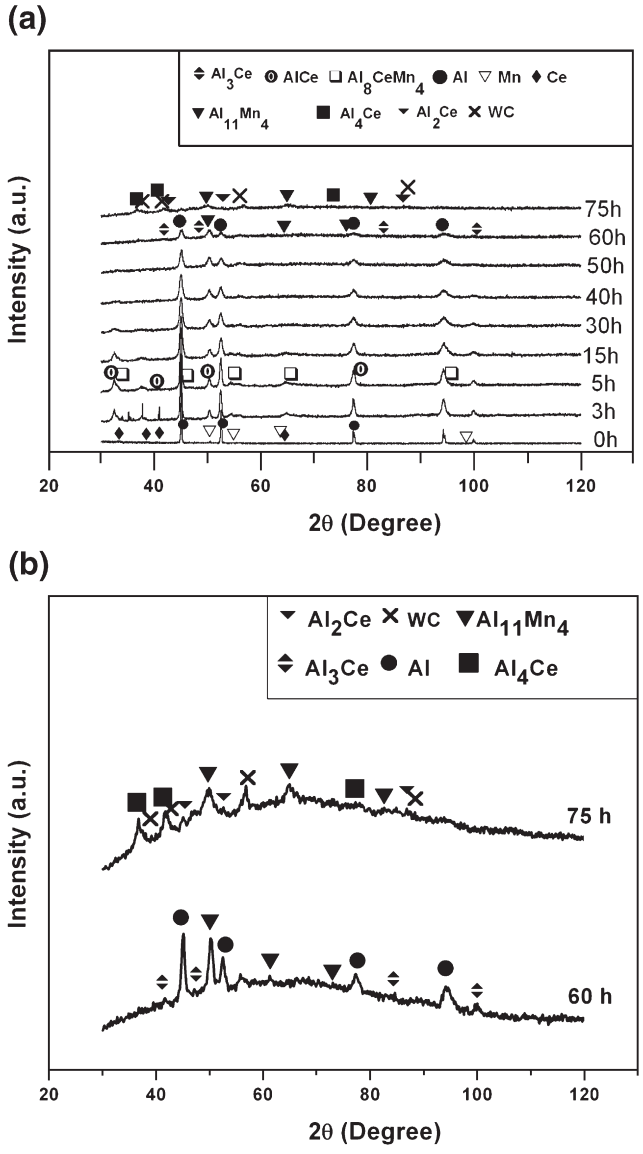

Fig. 1. (a) Modulation of XRD patterns of $Al_{92}Mn_6Ce_2$ with the progress of MA and (b) enlarged view of the same patterns for 60 and 75 h of MA.

intermetallic compounds of Al, Mn and Ce, namely, AlCe and Al_8CeMn_4, which were formed during the early stage of milling (3–15 h), gradually disappeared on further milling, and a different set of intermetallic compounds like Al_3Ce, and $Al_{11}Mn_4$ appeared at the later stage of MA (Fig. 1(a)). The enlarged view of the XRD patterns of the same composition after 60 h and 75 h of MA is presented separately in Fig. 1(b) for better illustration of the phase evolution during prolonged milling. Here, after 60 h of milling the structure appeared to be substantially amorphous, as evidenced by the presence of a broad amorphous hump in the XRD pattern (Fig. 1(b)). After 75 h of milling some new intermetallic phases like Al_2Ce and Al_4Ce were found in the milled product (Fig. 1(b)). The complicated nature of the ball milling process, namely, the complexity and sequence of dissolution of the alloying elements in the matrix, and the stability of the phases under sustained deformation during the MA process [19–23] were possibly responsible for the formation and/or dissolution of different intermetallic compounds during milling. From Fig. 1(b) it appears that the dissolution of Mn and Ce in the Al matrix coupled with the structural defects induced during prolonged MA possibly promoted the partial amorphization in $Al_{92}Mn_6Ce_2$ composition. The XRD pattern of the powder milled for 60 h or more (Fig. 1(b)) shows the presence of traces of WC, which is readily detectable because of the high scattering power of WC. Nevertheless, it emerges from the present study that the phases generated in the $Al_{92}Mn_6Ce_2$ composition by MA were quite different from those reported for the RSP of the same composition [1].

In order to investigate the role of Ce in the present alloy system, an elemental powder blend containing less amount of Ce, *i.e.*, $Al_{93}Mn_6Ce_1$ was mechanically alloyed, and the evolution of phases in course of its milling was monitored by XRD (Fig. 2(a)). The phases generated by MA in this case were somewhat different from those found in the higher Ce containing alloy. For instance, the intermetallic phases like Al_6Mn, Al_2Mn_3, Al_2Ce and Al_3Ce formed in the early stage of milling (3–15 h) of $Al_{93}Mn_6Ce_1$, and most of these phases (except Al_3Ce) were found to be stable even after 75 h of MA (Fig. 2(a)). But the intermetallic phases like $Al_{11}Mn_4$ and Al_4Ce, which were present in the $Al_{92}Mn_6Ce_2$ composition after 60 h of milling (Fig. 1(a)), were not found in the $Al_{93}Mn_6Ce_1$ alloy even after 75 h of MA. In case of $Al_{92}Mn_6Ce_2$ composition most of the phases forming in the early stage (3–15 h) of milling decomposed and/or dissolved with the progress of milling, whereas in lower Ce containing alloy mostly stable intermetallic phases were synthesized in the early stage of milling. This is basically due to the difference in Ce content, which seems to play an important role in the phase formation by MA in the Al–Mn–Ce system. The dissolution of the intermetallic phases, which were formed in the early stage of milling of $Al_{92}Mn_6Ce_2$, possibly resulted in the formation of partial amorphous structure in it with the progress of milling, as apparent from the presence of an amorphous hump in the XRD pattern (Fig. 1(b)).

It is interesting to note that the Ce content is the main difference between the two Al–Mn–Ce alloy compositions, and it exerted its influence even on the Ce-free intermetallic phases generated by MA, *viz.* $Al_{11}Mn_4$ formed in $Al_{92}Mn_6Ce_2$, whereas Al_6Mn and Al_2Mn_3 were found in $Al_{93}Mn_6Ce_1$. It may be noted that the alloy containing lower amount of Ce formed less number of Ce containing intermetallic compounds.

A magnified view of the XRD profiles after 60 h and 75 h of milling of $Al_{93}Mn_6Ce_1$ is presented separately in Fig. 2(b) for better illustration of the phase evolution in it. The absence of amorphous hump and the presence of peaks corresponding to WC can be clearly noticed in these XRD patterns. It is, therefore, evident that a completely crystalline structure was formed in the $Al_{93}Mn_6Ce_1$ composition after 75 h of MA (Fig. 2(b)) in contrast to the partial amorphization in $Al_{92}Mn_6Ce_2$ alloy (Fig. 1(b)). It may be pointed out that the XRD peak for WC in Fig. 1(b) appears to be much more prominent than that in Fig. 2(b), because the range of intensity involved in recording each crystalline pattern in Fig. 2(b) is about 2.5 times higher than that employed for recording individual amorphous based pattern in Fig. 1(b).

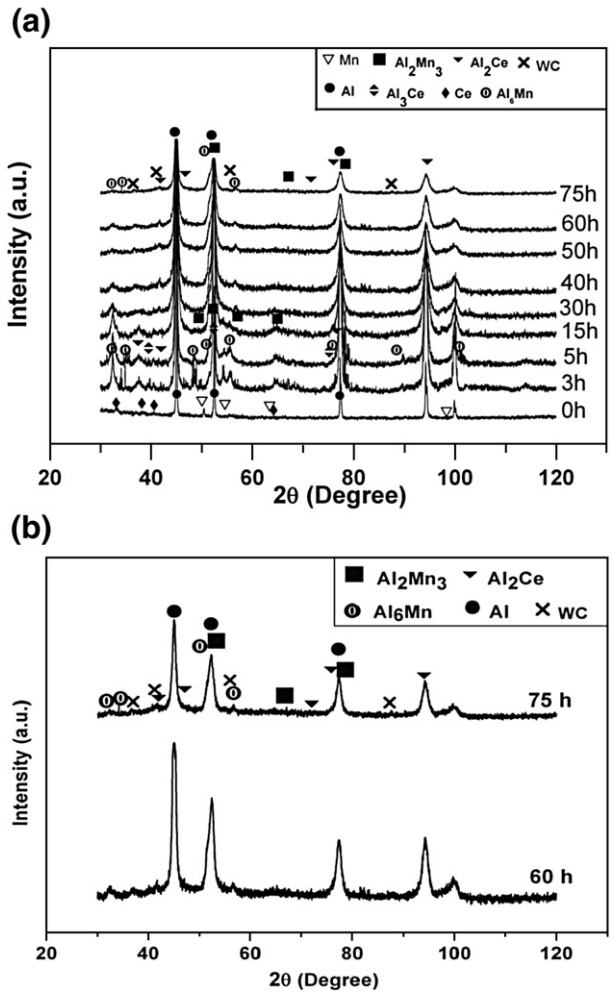

Fig. 2. (a) XRD patterns of $Al_{93}Mn_6Ce_1$ at different instances of MA, and (b) magnified view of the same patterns for 60 and 75 h.

It is known that small amount of impurities can trigger amorphization during ball milling [24,25]. For example, presence of 2.65 wt.% O in the milled powder along with C<0.05% resulted amorphization of Ti during ball milling [24]. In another case stable intermetallic phase Fe_2B could not be amorphized by mechanical grinding; but, an additional 4.2 wt.% Fe in the powder blend could yield amorphous structure by ball milling [25]. Hence, it is of interest to know the levels of contamination in the present compositions at the end of 75 h of ball milling. The XRD patterns in Figs. 1(b) and 2(b) show that some amount of WC contamination was present at this stage. The elemental analysis of both the alloys showed the presence of W~0.01 wt.% (in the form of WC), C<0.02 wt.% and O~0.08 wt.% as contamination in the powders after MA for 75 h. These levels are much smaller than the levels of impurity contamination/additions cited in the literature [24,25] for provoking the amorphous phase formation by ball milling. Hence, the presence of such a small level of contamination is unlikely to have any significant effect in the phase evolution during MA of $Al_{92}Mn_6Ce_2$ and $Al_{93}Mn_6Ce_1$. Moreover, in spite of the presence of similar level of contamination, entirely different types of structures were produced in $Al_{92}Mn_6Ce_2$ and $Al_{93}Mn_6Ce_1$ after prolonged milling under identical condition. Hence, it appears that the difference in Ce content in the two Al–Mn–Ce alloys played the pivotal role in the phase evolution during MA.

The XRD patterns in Figs. 1 and 2 indicate that the reduction in Ce content in the alloy from 2 to 1% remarkably diminished the amorphous phase formation. This result is in conformity with the electron diffraction (ED) patterns of the two alloys in Fig. 3. The ED pattern of 75 h milled sample of $Al_{92}Mn_6Ce_2$ in the inset of Fig. 3(a) shows a diffused halo due to the presence of amorphous phase, superimposed on the spotty patterns from the crystalline constituents. In contrast, the ED pattern of $Al_{93}Mn_6Ce_1$ alloy milled for the same duration in the inset of Fig. 3(b) displays only spotty rings, indicating predominantly crystalline nature of the phases generated in the alloy by MA.

Analysis of the XRD patterns of both the alloys, *i.e.*, $Al_{92}Mn_6Ce_2$ and $Al_{93}Mn_6Ce_1$, revealed that the crystallite size of Al-rich solid solutions initially decreased rapidly and attained almost a constant value of ~20 nm after 30 h of milling in both cases (Fig. 4). Fig. 3 displays the TEM images of the alloys of both compositions after prolonged milling (75 h). Here the average size of the particles is found to be of the order of 30 nm (Fig. 3), which is in reasonable agreement with the average crystallite size of the Al-rich solid solutions estimated by the XRD analysis (Fig. 4).

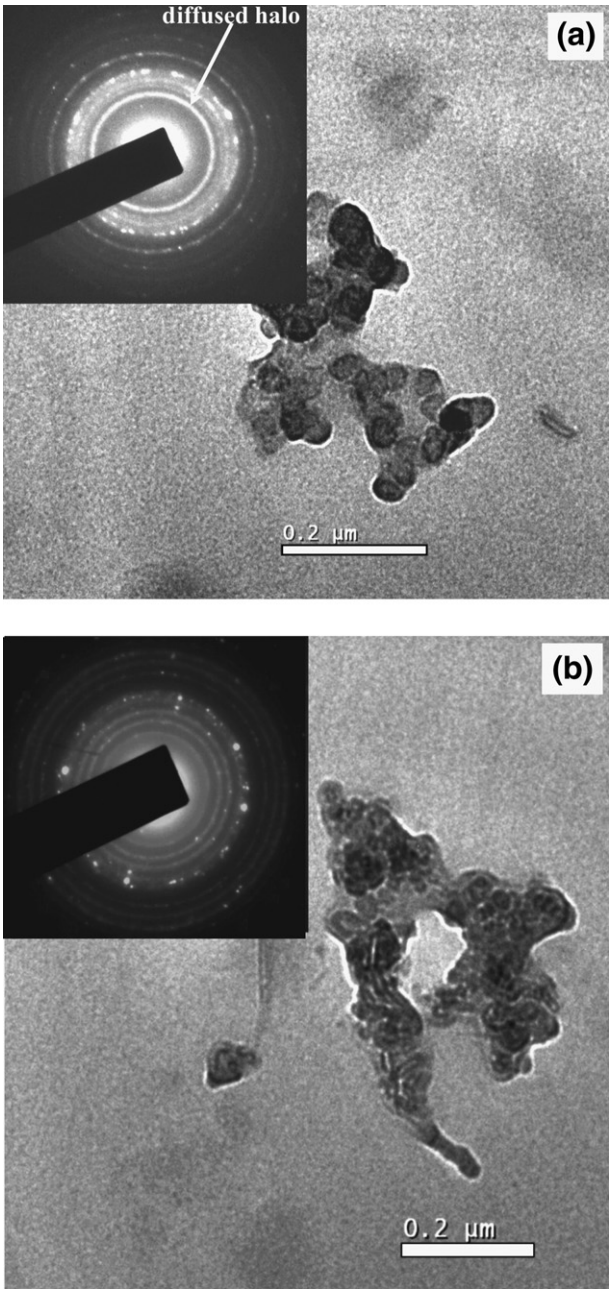

Fig. 3. Bright field TEM image and corresponding ED pattern (in the inset) of 75 h milled powders of (a) $Al_{92}Mn_6Ce_2$ and (b) $Al_{93}Mn_6Ce_1$.

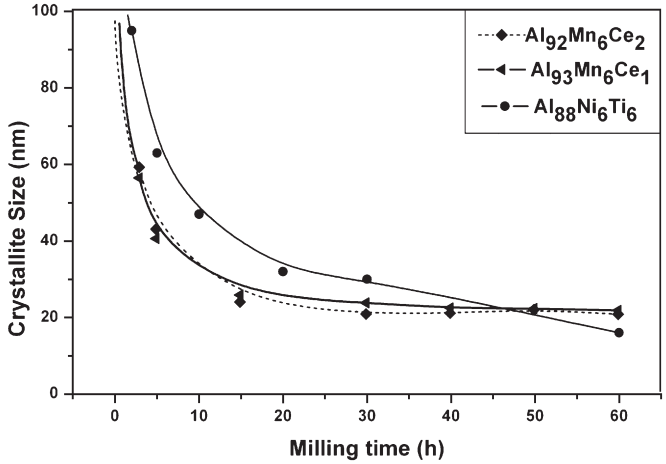

Fig. 4. Variation of crystallite size of Al-rich solid solution with milling time for $Al_{92}Mn_6Ce_2$, and $Al_{93}Mn_6Ce_1$ compared with that reported for $Al_{88}Ni_6Ti_6$ in [23].

In an exhaustive review, Eckert [26] has pointed out that it is very difficult to achieve complete amorphization during MA of an alloy containing more than 80 at.% Al, and often the structure shows coexistence of an amorphous phase and fcc Al-rich matrix with some intermetallic compounds [27–29]. The kinetic factors like competition between the amorphization and crystallization, and the structural factors like the extent of crystallite size refinement and strain energy stored in the milled product, the atomic size difference between the constituent elements, as well as, the stability of any intermetallic phase(s) under continued deformation can have a profound influence on the amorphization by MA. It is of interest to know, which of these factors has a dominant role in the amorphous phase formation during MA of the present alloy system.

In the present study, the lattice microstrain in both the Al–Mn–Ce alloys increased in a similar manner to nearly same level (~0.5%) during MA up to 60 h (Fig. 5). Thus, Fig. 4 along with Fig. 5 indicate that the excess energy stored in the milled products in the form of surface energy (due to the crystallite size refinement) and microstrain energy in both the Al–Mn–Ce alloys is of similar magnitude, and therefore, these factors cannot account for the diversity in structures of the as-milled products in these alloys. The variation of lattice parameter of the Al-rich solid solution (a_{Al}) during MA of these two alloys, however, showed a significant difference, as illustrated in Fig. 6. In both the alloys lattice parameter showed a decrease during the initial 15 h of milling, and thereafter it gradually increased up to 60 h of MA (Fig. 6).

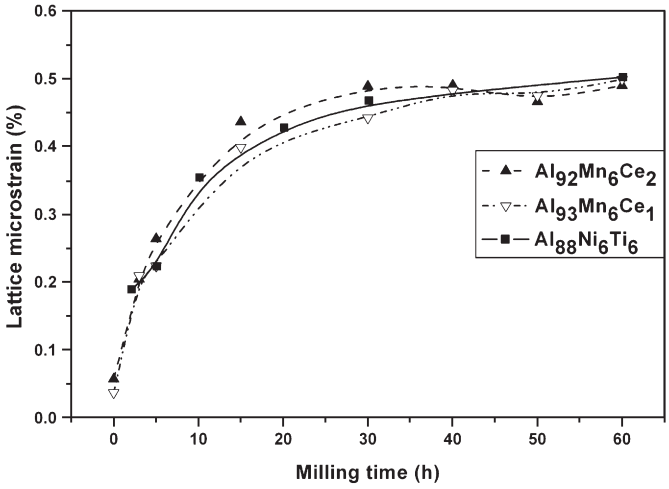

Fig. 5. Lattice microstrain (%) *vs.* milling time for $Al_{92}Mn_6Ce_2$, $Al_{93}Mn_6Ce_1$ and $Al_{88}Ni_6Ti_6$ (see text).

Since the atomic radius of Mn (0.118–0.134 nm) is less than that of Al (0.14318 nm) [30], Mn seems to enter into the solid solution of Al during the early stage of MA, and thereby causing a decrease in a_{Al}. On the other hand, the Ce (0.18244 nm) atoms are much bigger in size than the Al atoms, and the atomic size difference also exceeds 28%, which makes Ce almost insoluble in fcc-Al under equilibrium condition [30]. Therefore, the increase in lattice parameter during MA beyond 15 h (Fig. 6) may be attributed to the delayed dissolution of Ce in Al.

Fig. 6 shows that the extent of increase in lattice parameter with the progress of milling, after the initial decline, was more pronounced in the case of $Al_{92}Mn_6Ce_2$ as compared to that in $Al_{93}Mn_6Ce_1$ (*i.e.* lower Ce containing alloy). This factor was possibly instrumental in generating the partially amorphous structure in the $Al_{92}Mn_6Ce_2$ alloy. In order to verify this view, the variation of crystallite size and lattice parameter during MA of a fully amorphous phase forming Al-rich composition, *i.e.*, $Al_{88}Ni_6Ti_6$ recently reported by Das et al. [22,23] have been compared with the present alloys. The variation of lattice microstrain in $Al_{88}Ni_6Ti_6$ with the milling time was calculated from the experimental XRD data reported in [23], and the results are superimposed in Fig. 5. The results in Figs. 4 and 5 demonstrate that the variation of crystallite size and lattice microstrain with milling time (up to 60 h) in all the three Al-rich alloys are quite similar to each other. But the variation in lattice parameter is much more pronounced in the case of $Al_{88}Ni_6Ti_6$ (Fig. 6), which has also yielded a completely amorphous structure during MA, as compared to the partial amorphization achieved in the $Al_{92}Mn_6Ce_2$ milled under identical condition. Therefore, a wide variation in the lattice parameter of the Al-rich solid solution in the course of MA by addition of appropriate type and quantity of the alloying elements seems to be of profound importance in the design of amorphous forming composition. This view is in tune with the 'confusion principle' outlined by Inoue [15].

Rao [12] first postulated that an alloy with the smallest possible molar volume is most prone to the glass formation. Egami [13] discussed the theory of topological instability of the local atomic structure due to the atomic size difference, as well as, the concentration of these alloying additions to explain the solid state amorphization. The remarkable influence of the wide variation in lattice parameter of the Al-rich solid solution (Fig. 6) in the presence of similar level of interfacial and strain energy (*cf.* Figs. 4 and 5) indicated the dominant role of the said topological factors in the amorphous phase formation by MA. Naturally, any portion of these alloying additions utilized in the formation of intermetallic compounds is not

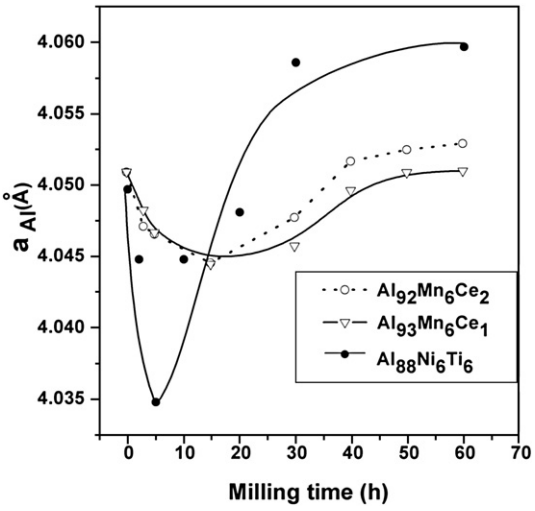

Fig. 6. Variation of lattice parameter of Al-rich solid solution, a_{Al}, with the progress of MA of $Al_{92}Mn_6Ce_2$ and $Al_{93}Mn_6Ce_1$ compared with that of $Al_{88}Ni_6Ti_6$ milled under identical condition and reported in [23].

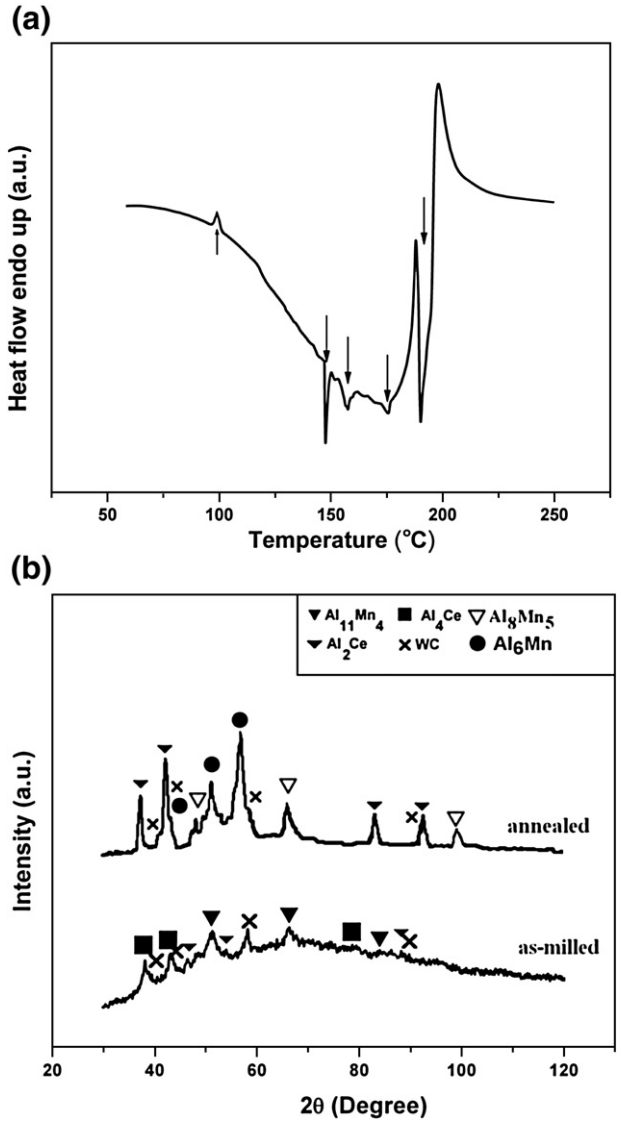

Fig. 7. (a) DSC thermogram of $Al_{92}Mn_6Ce_2$ milled for 75 h, recorded during heating at a rate of 5 °C/min under flowing helium atmosphere. (b) XRD patterns of 75 h milled sample before and after annealing at 250 °C for 2 h.

expected to contribute to the desired lattice parameter variation for the amorphous phase formation.

It may be recalled that the MA of $Al_{92}Mn_6Ce_2$ composition generated a structure that was completely different from that reported for RSP of the same composition [1]. This divergence in the product structure can originate from the difference in the mechanism of non-equilibrium phase formation in the two non-equilibrium processing routes. In RSP, all the alloying elements are in solution in the liquid prior to rapid solidification, and along with these the thermal disorders are frozen-in; whereas the sequence of dissolution of the different alloying elements and the level of mechanical disorders induced by the MA process can dictate the resultant phase evolution.

Fig. 7(a) depicts the thermal stability of the 75 h milled partially amorphous nanostructured product of $Al_{92}Mn_6Ce_2$ composition studied by DSC under flowing helium atmosphere. During DSC the temperature was raised up to 250 °C and the heating rate was 5 °C/min. First, an endothermic peak appeared at ~100 °C involving a small change of enthalpy (ΔH=0.61 J/g), which possibly was associated with the evaporation of adsorbents (like moisture) from the milled product. Thereafter, four prominent exothermic peaks appeared at ~148 °C (ΔH=−97 J/g), ~156 °C (ΔH=−32 J/g), ~175 °C (ΔH=−27 J/g) and ~190 °C (ΔH=−166 J/g), which were indicative of some phase transformation in the partially amorphous milled product. In order to get an insight into this event, the 75 h milled sample of $Al_{92}Mn_6Ce_2$ was annealed at 250 °C for 2 h, and then analyzed by XRD. The corresponding XRD pattern has been compared with that of the as-milled powder in Fig. 7(b). It shows a pronounced presence of the newly formed intermetallic compounds like Al_6Mn and Al_8Mn_5. This strong tendency of forming intermetallic compounds at relatively low temperatures (148 °C–190 °C) is not attractive for retaining the amorphous phase after sintering of this nanostructured powder. In contrast, Schwarz et al. [31] reported earlier that the icosahedral based structure produced by RSP of the same alloy, *i.e.*, $Al_{92}Mn_6Ce_2$ remained stable during the subsequent annealing at 550 °C for 1 h. This difference in the thermal stability may be attributed to the difference in the microstructure and strain in the products of MA and RSP. The presence of a high level of mechanical disorders in the milled product might have provoked easy decomposition of the metastable phases (*e.g.* amorphous phase) during subsequent annealing.

4. Conclusions

Phase evolution characteristics during mechanical alloying in $Al_{92}Mn_6Ce_2$ were quite different from that in $Al_{93}Mn_6Ce_1$, and it evidenced a strong influence of Ce even on the type of Ce-free intermetallic phase formation. The partial amorphization obtained in $Al_{92}Mn_6Ce_2$ during prolonged milling was not found in the lower Ce containing composition, *i.e.*, $Al_{93}Mn_6Ce_1$, thus indicating an important role of Ce in the formation of amorphous phase in Al–Mn–Ce system during MA.

The icosahedral based product structure reported for RSP of $Al_{92}Mn_6Ce_2$ was not obtained by MA of the same composition, possibly due to the difference in the alloying mechanism in these two non-equilibrium processing methods.

The wide variation in lattice parameter of the Al-rich solid solution in the presence of similar level of surface and strain energy stored in the milled products apparently indicated a pivotal role of the topological factors in the amorphous phase formation during MA of the present Al–Mn–Ce alloys.

The thermal stability of the metastable phases generated by MA was inferior to that reported for RSP of the same composition, *i.e.*, $Al_{92}Mn_6Ce_2$, possibly due to the difference in the product structure obtained through these two non-equilibrium processing routes.

References

[1] A. Inoue, Nanostruct. Mater. 6 (1995) 53–64.
[2] C. Suryanarayana, E. Ivanov, V.V. Boldyrev, Mater. Sci. Eng., A Struct. Mater.: Prop. Microstruct. Process. 304–306 (2001) 151–158.
[3] C.S. Kiminami, N.D. Basim, M.J. Kaufman, M.F. Amateau, T.J. Eden, G.J. Galbraith, Key. Eng. Mater. 89 (2001) 503–508.
[4] T. Masumoto, Mater. Sci. Eng., A Struct. Mater.: Prop. Microstruct. Process. 179–180 (1994) 8–16.
[5] F. Wu, P. Bellon, A.J. Melmed, T. Lusby, Acta Mater. 49 (2001) 453–461.
[6] J. Xu, G.S. Collins, L.S.J. Peng, M. Atzmon, Acta Mater. 47 (1999) 1241–1253.
[7] M.S. El-Eskandarany, M. Matsushita, A. Inoue, J. Alloys Compd. 329 (2001) 239–252.
[8] C. Gente, M. Oehring, R. Bormann, Phys. Rev., B 48 (1993) 13244–13253.
[9] A.R. Yavari, P.J. Desre, Mater. Sci. Eng., A Struct. Mater.: Prop. Microstruct. Process. 134 (1991) 1315–1322.
[10] F. Cardellini, G. Mazzone, M. Vittori Antisari, Acta Mater. 44 (1996) 1511–1517.
[11] J. Latuch, T. Kulik, H. Dimitrov, Mater. Sci. Eng., A Struct. Mater.: Prop. Microstruct. Process. 375–377 (2004) 956–960.
[12] P. Ramchandra Rao, Z. Met.kd. 71 (1980) 172–177.
[13] T. Egami, Mater. Sci. Eng., A Struct. Mater.: Prop. Microstruct. Process. 226–228 (1997) 261–267.
[14] A. Inoue, Prog. Mater. Sci. 43 (1998) 365–520.
[15] A. Inoue, Bulk amorphous alloys—preparation and fundamental characteristics, Mater. Sci. Found. 4 (1998) p.1 (Trans. Tech., Netherlands).
[16] L. Shaw, M. Zawrah, J. Villegas, H. Luo, D. Miracle, Metall. Mater. Trans., A Phys. Metall. Mater. Sci. 34A (2003) 159–170.
[17] B.D. Cullity, Elements of X-ray Diffraction, 2nd EditionAddison Wesley, Reading, MA, 1978 350 pp.
[18] T.H. Keijser, J.I. Langford, E.J. Mittemeijer, A.B.P. Vogels, J. Appl. Cryst. 15 (1982) 308–314.
[19] S.K. Pabi, D. Das, T.K. Mahapatra, I. Manna, Acta Mater. 46 (1998) 3501–3510.

[20] D. Das, P.P. Chatterjee, I. Manna, S.K. Pabi, Scripta Mater. 41 (1999) 861–866.
[21] M.K. Datta, S.K. Pabi, B.S. Murty, J. Appl. Phys. 87 (2000) 8393–8400.
[22] N. Das, G.K. Dey, B.S. Murty, S.K. Pabi, Pramana-J. Phys. 65 (2005) 831–840.
[23] N. Das, M. Tech. Thesis. IIT, Kharagpur, 2005.
[24] Y.Y. Li, C. Yang, W.P. Chen, X.Q. Li, M. Zhu, J. Mater. Res. 22 (2007) 1927–1932.
[25] J. Balogh, L. Bujdoso, T. Kemeny, I. Vincze, J. Phys., Condens. Matter 9 (1997) L503–L508.
[26] J. Eckert, Structure formation and mechanical behavior of two-phase nanostructured materials, in: C.C. Koch (Ed.), Nanostructured Materials-Processing, Properties and Potential Applications, Noyes, New York, 2002, pp. 423–525.
[27] T. Benameur, A. Inoue, T. Masumoto, Mater. Trans., JIM 35 (1994) 451–457.
[28] T. Benameur, A. Inoue, T. Masumoto, Nanostruct. Mater. 4 (1994) 303–322.
[29] M. Seidel, J. Eckert, H.D. Bauer, L. Schultz, in: M.A. Otooni, R.W. Armstrong, N.J. Grant, K. Ishizaki (Eds.), Grain Size and Mechanical Properties — Fundamentals and Applications, Mater. Res. Soc. Symp. Proc., Materials Research Society, Warrendale, PA, 1995, p. 239.
[30] E.A. Brandes, G.B. Brook (Editor), Smithells Metals Reference Book. 7th Edition. 1992, pp 4–41, 4–42, 11–32.
[31] R.B. Schwarz, Y. He, Mater. Sci. Forum 235–238 (1997) 231–240.